Online ISSN 1848-3380, Print ISSN 0005-1144
ATKAFF 57(4), 902–921(2016)

Pankaj Dahiya, Pankaj Mukhija, Anmol Ratna Saxena, Yogendra Arya

Comparative performance investigation of optimal controller for AGC of electric power generating systems

DOI 10.7305/automatika.2017.12.1707
UDK 681.537.015.24-047.44:621.31.011.752.016.22.078

Original scientific paper

In this study, an attempt is made to present the application and comparative performance analysis of optimal control approach for automatic generation control (AGC) of electric power generating systems. Optimal controller is designed utilizing performance index minimization criterion. To conduct the study, various single and multi-area models with/without system nonlinearities from the literature are simulated under sudden load perturbation. In this comparative study, to corroborate the worth of optimal controller, the performance of optimal AGC controller is compared with that of I/PI controller optimized adopting recently published the best established techniques such as teacher learning based optimization (TLBO), differential evolution (DE), genetic algorithm (GA), particle swarm optimization (PSO), hybrid bacteria foraging optimization algorithm-PSO (hBFOA-PSO), craziness based PSO (CBPSO), firefly algorithm (FA), krill herd algorithm (KHA), moth-flame optimization (MFO), glow swarm optimization (GSO), simulated annealing (SA), bat algorithm (BA), stochastic fractal search (SFS) and hybrid SFS-local unimodal sampling (hSFS-LUS) technique. The simulated results are compared in terms of settling time (ST), peak undershoot (PU)/overshoot (PO), various performance indices (PIs), minimum damping ratio ($\xi_{\min}$) and system eigenvalues. A sensitivity study is conducted to certify the robustness of optimal controller.

Key words: Automatic generation control, Multi-source power system, Sensitivity analysis, Frequency regulation, Optimal control applications

Komparativna analiza primjene optimalnog upravljanja za automatsko upravljanje sustavima za proizvodnju električne energije. U ovom radu se razmatra primjena i komparativna analiza sustava za automatsko planiranje proizvodnje proizvođača električne energije. Sinteza optimalnog regulatora proporcionalno-integralne strukture je provedena korištenjem integralnih kriterija. Različiti modeli s jednim područjem i više područja te s i bez nelinearnosti korišteni su u simulaciji nagle promjena opterećenja. Kako bi se pokazala važnost optimalnog regulatora, u komparativnoj analizi su performanse dizajniranog optimalnog regulatora uspoređene s peformansama postignutim korištenjem I i PI regulatora sintetiziranih primjenom postojećih uobičajeno korištenih metoda kao što su *teacher learning optimization*, diferencijska evolucija, genetski algoritam, optimizacija rojem čestica, *hybrid bacteria foraging* optimizacijski algoritam, *craziness based* optimizacija rojem čestica, *firefly* algoritam, *krill herd* algoritam, *moth-flame* optimizacija, *glow swarm* optimizacija, metoda simuliranog kaljenja, *bat* algoritam, stohastično fraktalno traženje (eng. *stochastic fractal search*,SFS) i metoda hibridnog SFS lokalnog unimodalnog uzorkovanja. Performanse primijenjenih algoritama upravljanja vrednovani su usporedbom ostvarenih vremena ustaljivanja, iznosa podbačaja i prebačaja te drugih pokazatelja performansi, minimalnih relativnih koeficijentima prigušenja i svojstvenih vrijednosti sustava upravljanja. Provedena analiza osjetljivosti potvrđuje robusnost parametara optimalnog regulatora za širok raspon radnih točaka i parametara sustava.

Ključne riječi: automatizacija proizvodnje, elektroenergetski sustav s više izvora,analiza osjetljivosti,regulacija frekvencije,primjena optimalnog upravljanja

1 INTRODUCTION

Modern electrical power system comprises of an interconnection of numerous control areas. Interconnected power system is imperative to improve the reliability of the system, preserve the power supply continuity and share the spinning reserve. For consistent operation of an electric power system, the maintenance of constant generation, frequency and tie-line power flow is an utmost important issue [1]. The imbalance between generation and demand of power takes place due to random changes in the load demands. Automatic generation control (AGC) performs incessant task of real-time adjustment of power generation economically via employing a suitable control strategy and

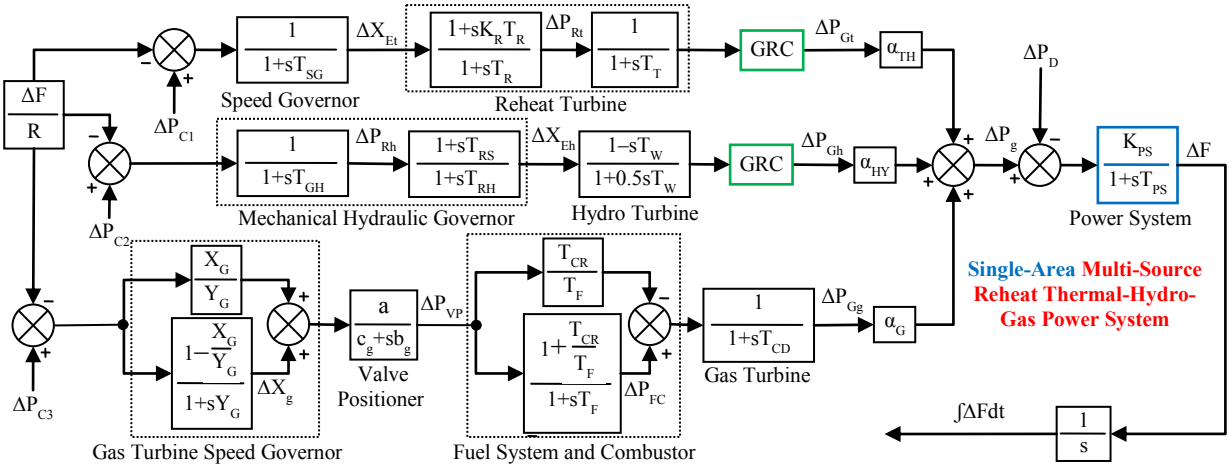

Fig. 1. Transfer function model of single-area multi-source hydrothermal gas power system.

hence supply quality electric power with sufficient degree of system security to the end users. The prime purpose of AGC is to preserve the system frequencies as close as possible to the particular nominal value and to maintain the correct value of power flow over the tie-lines interconnecting the control areas by maintaining area control error (ACE), which is the linear combination of deviation in tie-line power and deviation in frequency, to zero. The tie-lines in addition to act as medium to exchange contractual power between areas, offer inter-area support in case of abnormal conditions [2].

Over the recent past years, a large number of evolutionary soft computational intelligent strategies have emerged and implemented to optimize and also act as various types of supplementary controllers in AGC study of power systems as reviewed extensively in [2–3]. The various intelligent control techniques appeared recently in the literature like differential evolution (DE) based PI/PID [4], teaching learning based optimization (TLBO) based 2-DOF PID [5], backtracking search algorithm (BSA)/fruit fly algorithm (FFA) based PID [6], bacteria foraging optimization algorithm (BFOA)/particle swarm optimization (PSO) algorithm/hybrid BFOA-PSO (hBFOA-PSO) algorithm based PI [7], craziness based PSO (CBPSO) based PI [8], firefly algorithm (FA) based I/PI/ID/PID [9], glow swarm optimization (GSO) based PI [10], stochastic fractal search (SFS)/hybrid SFS-local unimodal sampling (hSFA-LUS) based I/PID/multistage PID [11], moth-flame optimization (MFO) based I/PI/PID/IDD/PID+DD [12], improved PSO based fractional order PID (FOPID) [13], krill herd algorithm (KHA) based I/PI/PID/IDD/PIDD [14], quasi-oppositional harmony search (QOHS) algorithm based fuzzy PI/PD/PID (FPI/FPD/FPID) [15], imperialist competitive algorithm (ICA) based FO fuzzy PID (FOFPID) [16], BFOA based FPI/FPID [17], hybrid DE-PSO based FPID [18], CBPSO/real coded GA based I [19] and BFOA based PID/FPID/FOPID/FOFPID [20] controllers have been exploited to solve AGC problem of various types of single/multi-area power systems. However, these approaches may betray the desired solution sometime in worst operating condition [19].

The supplementary AGC controllers designed by utilizing modern artificial intelligent methods frequently do not give fix solution to AGC problem. Furthermore, classical controller design is normally restricted to single-input single-output systems. However, AGC controller design is a multivariable problem which may be justified effectively via the use of modern optimal control design method. Since the first attempt of Fosha and Elgerd [21], modern optimal control theory has appeared in the literature in a large range of research articles over about four decades [22–29]. After the investigation of these articles it is deduced that enhanced performance with superior stability margins is experienced with optimal control strategy in contrast to conventional control techniques. Further, optimal controller is more robust, economical and easy to design and implement in power system. Additionally, classical AGC controller usually shows comparatively large oscillations and settling time in the system dynamic responses in comparison to optimal AGC controller [25,27].

The present study tries to showcase the benefits of optimal controller over classical I/PI controller tuned using various soft computing techniques appeared recently in the literature for AGC of various single and multi-area power systems with and without system nonlinearities. Moreover, the current study is the extension of the work done in [27]. Consequently, the main objective and contribution of the present work is to frame optimal controller based on full state vector feedback control strategy employing performance index minimization criterion and to demon-

strate its advantages over I/PI controller optimized via TLBO, DE, GA, PSO, hBFOA-PSO, CBPSO, FA, KHA, BA, MFO, GSO, SA, BA, SFS and hSFS-LUS techniques. The supremacy of optimal controller over the techniques stated above is demonstrated in terms of least numerical values of settling time (ST)/peak undershoot (PU)/peak overshoot (PO)/performance indices (PIs), higher values of $\xi_{\min}$ and the presence of real part of system eigenvalues more in the left half of s plane. Finally, a sensitivity analysis is conducted to confirm the robustness of optimal controller parameters under wide changes in the initial loading condition and important parameters of the system from the nominal values.

2 SYSTEMS UNDER INVESTIGATION

In this comparative performance study, investigations are carried out on different six AGC system models such as single-area multi-source hydrothermal gas power system with generation rate constraint (GRC) as given in Fig. 1, two-area non-reheat thermal power system as shown in Fig. 2, two-area non-reheat thermal power system with governor deadband (GDB) nonlinearity as shown in Figs. 2-3, two-area reheat thermal power system as shown in Fig. 4, two-area hydrothermal power system with GDB/GRC as shown in Ref. [10] and three-area reheat thermal power system as shown in Fig. 5. In single-area system, multiple diverse source power plants like thermal, hydro and gas operate. In hydrothermal power system, area-1 has hydro plant and area-2 has thermal plant. The power rating of each control area of single/two-area system is 2000 MW, however, power ratings of three-area system is 2000 MW, 5000 MW and 8000 MW for area-1, 2 and 3, respectively. The nominal values of system parameters are presented in Appendix. The different states/symbols used in Figs. 1-5 are explained in the nomenclature table.

3 STATE SPACE MODELS

The transfer function diagrams of single, two and three-area power system models under investigation are shown in Figs. 1–5. As per the states shown in these figures, the state (X), control (U) and disturbance (P_d) vectors for different system models are selected as follows:

- State vectors
  Single-area multi-source hydrothermal gas power system model:

$$[X]^{\mathrm{T}} = [\Delta F\ \Delta\ P_{\mathrm{Gt}}\ \Delta P_{\mathrm{Rt}}\ \Delta X_{\mathrm{Et}}\ \Delta P_{\mathrm{Gh}}\ \Delta X_{\mathrm{Eh}} \ldots \Delta P_{\mathrm{Rh}}\ \Delta P_{\mathrm{Gg}}\ \Delta P_{\mathrm{FC}}\ \Delta P_{\mathrm{VP}}\ \Delta X_{\mathrm{g}}\ \int Fdt] \quad (1)$$

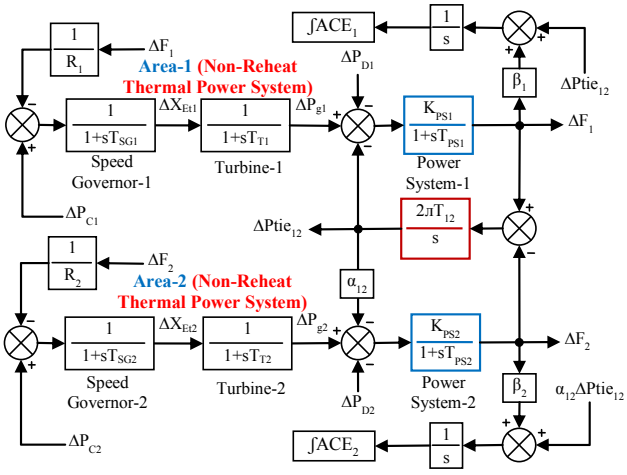

Fig. 2. Transfer function model of two-area non-reheat thermal power system.

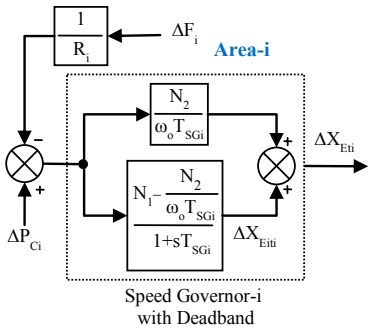

Fig. 3. Speed governor with deadband nonlinearity of area-i.

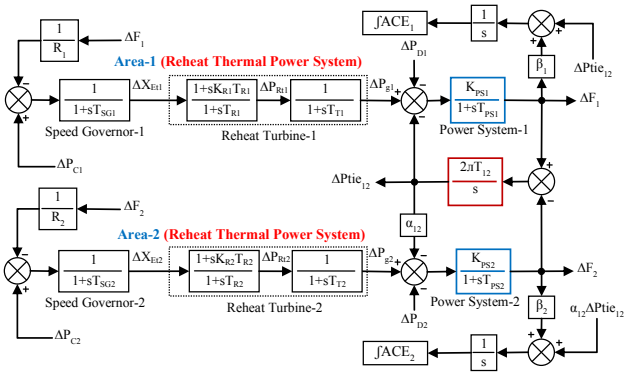

Fig. 4. Transfer function model of two-area reheat thermal power system.

Two-area non-reheat thermal power system model:

$$[X]^{\mathrm{T}} = [\Delta\ Ptie_{12}\ \Delta F_1\ \Delta P_{\mathrm{g1}}\ \Delta X_{Et1} \ldots \int ACE_1 dt \Delta F_2\ \Delta P_{g2}\ \Delta X_{Et2}\ \int ACE_2 dt], \quad (2)$$

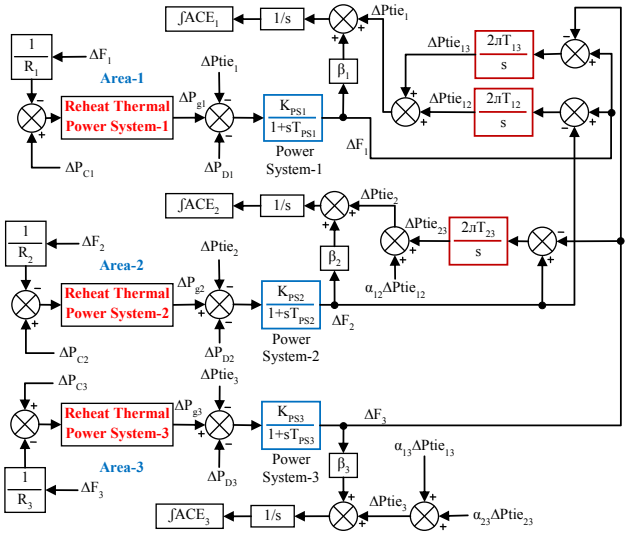

Fig. 5. Transfer function model of three-area reheat thermal power system.

Two-area non-reheat thermal power system with GDB model:

$$[X]^{\mathrm{T}} = [\Delta Ptie_{12}\ \Delta F_1\ \Delta P_{g1}\ \Delta X_{Eit1} \ldots \int ACE_1 dt\ \Delta F_2\ \Delta P_{g2}\ \Delta X_{Eit2}\ \int ACE_2 dt], \tag{3}$$

Two-area reheat thermal power system model:

$$[X]^{\mathrm{T}} = [\Delta Ptie_{12}\ \Delta F_1\ \Delta P_{g1}\ \Delta P_{Rt1}\ \Delta X_{Et1} \ldots \int ACE_1 dt\ \Delta F_2\ \Delta P_{g2}\ \Delta P_{Rt2} \ldots \Delta X_{Et2}\ \int ACE_2 dt], \tag{4}$$

Two-area hydrothermal power system model:

$$[X]^{\mathrm{T}} = \left[\int ACE_1 dt\ \Delta F_1\ \Delta P_{g1}\ \Delta X_{Eh}\ \Delta P_{Rh} \ldots \Delta Ptie_{12}\ \int ACE_2 dt\ \Delta F_2\ \Delta P_{g2}\ \Delta P_{Rt}\ \Delta X_{Et}\right], \tag{5}$$

Three-area reheat thermal power system model:

$$[X]^{\mathrm{T}} = [\Delta F_1\ \Delta F_2\ \Delta F_3\ \Delta Ptie_{12}\ \Delta Ptie_{13} \ldots \Delta Ptie_{23}\ \Delta P_{g1}\ \Delta P_{g2}\ \Delta P_{g3}\ \Delta P_{Rt1}\ \Delta P_{Rt2} \ldots \Delta P_{Rt3}\ \Delta X_{Et1}\ \Delta X_{Et2}\ \Delta X_{Et3}\ \int ACE_1 dt \ldots \int ACE_2 dt\ \int ACE_3 dt], \tag{6}$$

- Control vectors

  Single-area multi-source hydrothermal gas/three-area reheat thermal power system model:

$$U = [\Delta P_{C1}\ \Delta P_{C2}\ \Delta P_{C3}]^{\mathrm{T}} \tag{7}$$

  Two-area non-reheat/non-reheat with GDB/reheat/hydrothermal power system model:

$$U = [\Delta P_{C1}\ \Delta P_{C2}]^{\mathrm{T}} \tag{8}$$

- Disturbance vectors

  Single-area multi-source hydrothermal gas power system model:

$$\mathrm{P_d} = [\Delta P_D] \tag{9}$$

  Two-area non-reheat/non-reheat with GDB/reheat/hydrothermal power system model:

$$\mathrm{P_d} = [\Delta P_{D1}\ \Delta P_{D2}]^{\mathrm{T}} \tag{10}$$

  Three-area reheat thermal power system model:

$$\mathrm{P_d} = [\Delta P_{D1}\ \Delta P_{D2}\ \Delta P_{D3}]^{\mathrm{T}} \tag{11}$$

4 DESIGN OF OPTIMAL CONTROLLER

The controllable and observable linear time-invariant state-space representation of power system models under study can be expressed by the following differential equations:

$$\dot{X} = AX + BU + \Gamma P_d, \tag{12}$$

$$Y = CX, \tag{13}$$

where X, U, $\mathrm{P_d}$ and Y are the state, control, disturbance and output vectors, respectively. A, B, C and Γ are system, control, output and disturbance matrices of appropriate dimensions, respectively.

To design optimal controller for the system expressed by equations (12) and (13), a full state vector feedback control law of the form of (14) is to be computed via minimization of a quadratic cost function or performance index J given by (15).

$$U^* = -K^* X. \tag{14}$$

$$J = \int_0^\infty \frac{1}{2}[X^{\mathrm{T}} Q X + U^{\mathrm{T}} R U]dt. \tag{15}$$

In (15), Q and R are the positive semi-definite symmetric state and positive definite symmetric control cost weighting matrices of appropriate dimensions, respectively. The Q and R must assure the definiteness conditions as: $Q \geq 0$ and $R > 0$.

In the implementation of optimal control theory, the term ΓP_d in (12) is removed by redefining the states and

controls in terms of their post disturbance steady state values. However, (13) will not change but (12) can be rescripted as:

$$\begin{aligned} \dot{X} &= AX + BU + \Gamma P_d \\ X(0) &= X_0. \end{aligned} \tag{16}$$

For the infinite time problem, the implementation of Pontryagin's minimum principle gives the following continuous time algebraic matrix Riccati equation [30]:

$$PA + A^{\mathrm{T}}P - PBR^{-1}B^{\mathrm{T}}P + Q = 0. \tag{17}$$

The solution of (17) provides a positive definite symmetric matrix, P. In (14) the feedback gain matrix K^*, which minimizes (15) is computed via the solution of (17) as:

$$K^* = R^{-1}B^{\mathrm{T}}P \tag{18}$$

The K^* matrices are computed using MATLAB software for each system and are provided in subsections 5.1-5.6 with their dimensions. The design of optimal controller is obtained using state feedback theory as reported in the literature [1,21–29]. The matrices A, B, C, Γ, Q and R and vector X, U and P_d are required to design an optimal controller for the corresponding power system. For single-area multi-source hydrothermal gas system, the sizes of matrices A, B, C, Γ, Q and R are [12×12], [12×3], [12×12], [12×1], [12×12] and [3×3] and the sizes of vectors X, U and P_d are [12×1], [3×1] and [1×1], respectively. For two-area non-reheat thermal system with/without GDB, the sizes of matrices A, B, C, Γ, Q and R are [9×9], [9×2], [9×9], [9×2], [9×9] and [2×2] and the sizes of vectors X, U and P_d are [9×1], [2×1] and [2×1], respectively. For two-area reheat thermal/hydrothermal system, the sizes of matrices A, B, C, Γ, Q and R are [11×11], [11×2], [11×11], [11×2], [11×11] and [2×2] and the sizes of vectors X, U and P_d are [11×1], [2×1] and [2×1], respectively. For three-area reheat thermal system, the sizes of matrices A, B, C, Γ, Q and R are [18×18], [18×3], [18×18], [18×3], [18×18] and [3×3] and the sizes of vectors X, U and P_d are [18×1], [3×1] and [3×1], respectively.

In the current work, R is selected as identity matrix and Q is based on minimum value of the performance index for all the power system models under investigation [29]. The state space matrices A, B, C and Γ of compatible dimensions are acquired by arranging state space differential equations written for all six power system models under study. The various differential equations and the state space A, B, C and Γ matrices are not given in the paper to save the pages. However, the vectors X, U and P_d for all six power system models under study are provided in Eqns. (1)-(11).

5 SIMULATION RESULTS AND DISCUSSIONS

The state space models of the power systems under study written in .mfiles in MATLAB environment are simulated using the system data given in Appendix. Because of the fact that the settling times (STs) of simulation results should be defined in a tolerance band, STs in the present work are obtained in a tolerance band of ± 0.0005 for all the systems. Additionally, as the error values of various performance indices (PIs) should be calculated for a specified time of simulation, PIs are calculated for a simulation time of 25 s for all the power system models. The results of attention are shown bold faced in the individual comparative tables of responses. The subsequent sections describe the simulation outcomes of the various types of power system models under investigation.

5.1 Single-area multi-source hydrothermal gas system

The transfer function model of single-area multi-source hydrothermal gas power system is shown in Fig. 1. The thermal plant is equipped with reheat type turbine having open loop GRC nonlinearity of ± 0.1 pu/s [10,20] and hydro plant equipped with mechanical governor has open loop GRC nonlinearity of $+0.045$ pu/s and -0.06 pu/s [17,20,22]. Electric power plant cannot change its output too quickly due to the restriction imposed by the thermal and mechanical movements. Thus, constraints operate on the rate of change of generation termed as generation rate constraint (GRC). Hence, GRC must be incorporated for a realistic AGC study. To avoid system instability, an appropriate supplementary controller should be used in the system. Hence, to check the suitability of optimal controller, GRC is used in the system. The state, control and disturbance vectors for the system are given in Eqns. (1), (7) and (9), respectively. The optimal feedback gain matrix K^* of optimal controller having size [3×12] obtained for single-area multi-source hydrothermal gas system is stated as follows:

$$K^* = \begin{bmatrix} 1.2334 & 1.0517 & 2.6042 & \cdots \\ -0.1732 & -0.0579 & 0.5907 & \cdots \\ 0.5660 & 0.5089 & 1.1846 & \end{bmatrix}$$

$$\begin{matrix} -0.6879 & 0.9136 & 1.4236 & 0.0732 & \\ -0.1760 & -0.0124 & 0.4170 & -0.0536 & \cdots \\ -0.3100 & 0.4531 & 0.5698 & 0.0654 & \end{matrix}$$

$$\begin{bmatrix} 0.1795 & 0.1775 & 0.0368 & 0.3141 & 0.9074 \\ -0.0148 & -0.0011 & 0.0006 & 0.0669 & -0.1154 \\ 0.0854 & 0.0885 & 0.0186 & 0.1728 & 0.4041 \end{bmatrix}$$

The system is simulated by employing these feedback gains for a 5% step load perturbation (SLP) in the area

applied at $t = 0$ s. The frequency deviation (ΔF) and area power generation (ΔP_g) response characteristics of the system are shown in Figs. 6a-b. To confirm the advantage of optimal controller, the results due to it are compared with integral (I) controller optimized via recently developed intelligent optimization techniques like stochastic fractal search (SFS) and hybrid SFS-local unimodal sampling (hSFS-LUS) [11]. It can be seen from Figs. 6a-b that optimal controller displays better dynamic performance in comparison to other two controllers in terms of lesser peak overshoot (PO)/peak undershoot (PU)/settling time (ST) and smooth/fast responses.

Table 1. Comparative performance analysis of single-area multi-source system.

Controllers	Parameter	Optimal controller	hSFS-LUS: I [11]	SFS: I [11]
ST	ΔF	**6.9100**	14.5800	13.9800
PO	ΔF	**0.0000**	0.0268	0.0187
PU	ΔF	**-0.1869**	-0.3241	-0.3260
PIs	ISE	**0.0489**	0.2190	0.2254
	ITSE	**0.0622**	0.4295	0.4469
	IAE	**0.3752**	0.9585	0.9672
	ITAE	**0.6092**	2.3750	2.3440
$\xi_{\min}$		**0.6896**	0.4944	0.5069
Eigenvalues		-19.9786	-19.9794	-19.9794
		-12.6502	-12.5000	-12.5000
		-5.8719	-5.6625	-5.6654
		-5.0000	-5.0000	-5.0000
		-3.9380	-3.6394	-3.6340
		-2.8249	-2.0000	-2.0000
		-1.2817	-3.3333	-3.3333
		-1.1916	-0.1359	-0.1436
		$\pm$ 1.2513i	$\pm$ 0.4414i	$\pm$ 0.4268i
		-0.7476	-0.8817	-0.8688
		-0.0394	-0.0348	-0.0348
		-0.2631	-0.1000	-0.1000

To enhance the clarity, the system simulation responses are also given in Table 1 in terms of numerical values of ST, PO, PU, minimum damping ratio ($\xi_{\min}$), system eigenvalues and various types of performance indices (PIs) like integral of squared error (ISE), integral of time multiplied squared error (ITSE), integral of absolute error (IAE), and integral of time multiplied absolute error (ITAE) for ΔF state. The critical investigation of Table 1 reveals that optimal controller exhibits better dynamic performance having least ST (6.91 s), PO (0 Hz), PU (–0.1869 Hz), ISE (0.0489), ITSE (0.0622), IAE (0.3752), ITAE (0.6092) and greater $\xi_{\min}$ (0.6896) in comparison to SFS/hSFS-LUS tuned I controller [11]. It should be noted that for a healthier, stable and controlled system, $\xi_{\min}$ value should be high [7,27]. It is also observed from Table 1 that most of the eigenvalues of the system with optimal controller have higher negative real parts in comparison to optimized I controllers. Hence, system with optimal controller exhibits substantially higher stability margins with good damping due to which a superior performance is observed with it.

5.2 Two-area non-reheat thermal power system

The transfer function model of two-equal area non-reheat thermal power system is shown in Fig. 2. The state, control and disturbance vectors for the system are given in Eqns. (2), (8) and (10), respectively. For two-area non-reheat thermal system, optimal controller parameters i.e., K^* matrix with [2×9] dimension are given as follows:

$$K^* = \begin{bmatrix} -0.1773 & 0.4246 & 0.6615 & 0.1628 & \cdots \\ 0.1773 & -0.0789 & -0.1148 & -0.0263 & \cdots \end{bmatrix}$$
$$\begin{matrix} 1 & -0.0789 & -0.1148 & -0.0263 & 0 \\ 0 & 0.4246 & 0.6615 & 0.1628 & 1 \end{matrix} \Bigg]. \quad (19)$$

The simulation results of deviation in frequency of area-1 (ΔF_1), deviation in frequency of area-2 (ΔF_2) and deviation in tie-line power flow ($\Delta Ptie_{12}$) system states with optimal controller under simultaneous big 10% SLP in area-1 and 20% SLP in area-2 at $t = 0$ s are displayed in Figs. 7a-c.

The values of various performance parameters such as ST, PO, PU etc., are stated in Table 2. To confirm the benefit of optimal controller, responses of the lately published and the best claimed GA/PSO/hBFOA-PSO [7] and TLBO [5] based PI controller for the same power system are also incorporated in Figs. 7a-c and Table 2. Critical scrutiny of Figs. 7a-c clearly discloses that the system dynamic responses with the designed optimal controller are non-oscillatory, smooth and settle to the desired zero value hastily. It is also apparent from Table 2 that, minimum ITAE (2.078), IAE (1.287), ITSE (0.2431) and ISE (0.2552) values are obtained with optimal controller compared to GA, PSO, hBFOA-PSO and TLBO tuning methods based PI controller. It is also clear from Table 2 that, system performance gets better with optimal control strategy having noteworthy higher $\xi_{\min}$ (0.3077) and reduced ST ($\Delta F_1 = 9.91$ s, $\Delta F_2 = 9.51$ s and $\Delta Ptie_{12} = 7.55$ s), PO ($\Delta F_1 = \Delta F_2 = 0$ Hz and $\Delta Ptie_{12} = 0.0502$ puMW) and PU ($\Delta F_1 = -0.3152$ Hz, $\Delta F_2 = -0.4179$ Hz and $\Delta Ptie_{12} = 0$ puMW) values over other PI controllers. Additionally, all system eigenvalues with optimal controller are most favorable. The better values are bold faced in Table 2. Consequently, optimal controller in all respect, demonstrates superior performance over GA/PSO/hBFOA-PSO/TLBO tuned PI controller.

5.3 Two-area non-reheat thermal power system with GDB

An attempt is made to design optimal controller using state space model of a two-area non-reheat thermal AGC

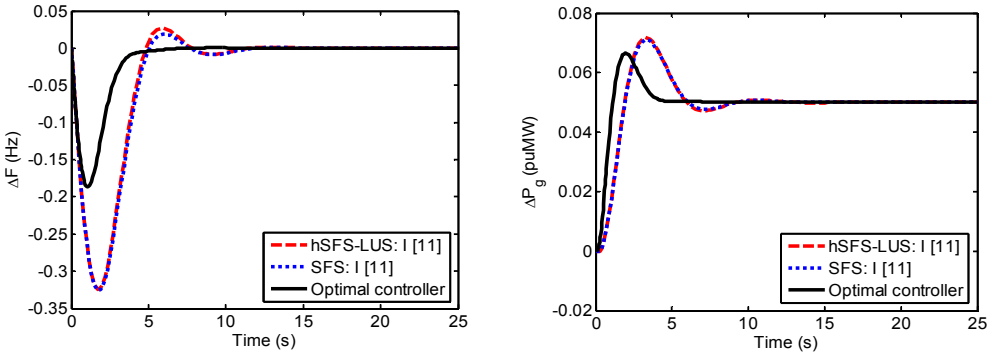

(a) (b)

Fig. 6. Comparative dynamic responses offered by optimal controller for single-area multi-source hydrothermal gas system with 5% SLP in the area at $t = 0$ s (a) ΔF vs. Time and (b) ΔP_g vs. Time.

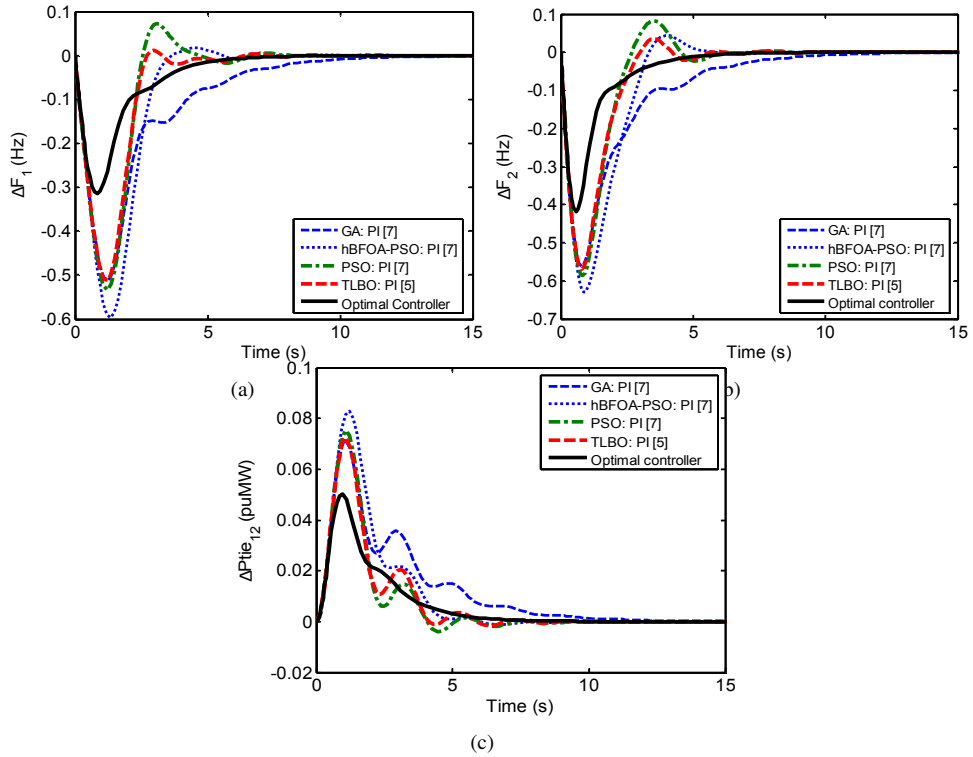

(a) (b)

(c)

Fig. 7. Comparative dynamic responses offered by optimal controller for two-area non-reheat thermal system with simultaneously 10% SLP in area-1 and 20% SLP in area-2 at $t = 0$ s (a) ΔF_1 vs. Time (b) ΔF_2 vs. Time and (c) $\Delta Ptie_{12}$ vs. Time.

Table 2. Comparative performance analysis of two-area non-reheat thermal system.

Parameters		Optimal Controller	TLBO: PI [5]	PSO: PI [7]	hBFOA-PSO: PI [7]	GA: PI [7]
PIs	ITAE	**2.0780**	2.5010	2.9510	3.7250	7.1580
	IAE	**1.2870**	1.8040	1.9560	2.4150	2.8400
	ITSE	**0.2431**	0.6877	0.7738	1.2440	1.1540
	ISE	**0.2552**	0.6388	0.6942	0.9825	0.7933
ST	ΔF_1	**9.91**	10.13	10.53	10.81	16.55
	ΔF_2	**9.51**	10.09	9.86	10.78	16.20
	$\Delta Ptie_{12}$	**7.55**	8.62	7.76	9.06	12.09
PO	ΔF_1	**0.0000**	0.0125	0.0724	0.0171	0.0000
	ΔF_2	**0.0000**	0.0347	0.0828	0.0447	0.0000
	$\Delta Ptie_{12}$	**0.0502**	0.0725	0.0753	0.0829	0.0715
PU	ΔF_1	**-0.3152**	-0.5118	-0.5336	-0.5964	-0.5126
	ΔF_2	**-0.4179**	-0.5689	-0.5863	-0.6287	-0.5612
	$\Delta Ptie_{12}$	**0.0000**	-0.0015	-0.0398	-0.0011	0.0000
ξ_{min}		**0.3077**	0.1735	0.1887	0.2374	0.1740
Eigenvalues		**-13.2767**	-13.0760	-13.0375	-12.9969	-13.1203
		-13.3029	-13.0466	-12.9961	-12.9427	-13.1043
		-1.2262±3.7916i	-0.8699±0.4549i	-0.7635±1.5085i	-0.8772±1.2442i	-1.1751±1.9112i
		-1.7957±2.8755i	-0.9267±1.6635i	-0.8620±0.6179i	-0.7475±0.5089i	-0.5605±3.1716i
		-1.8002	-0.9832	-1.3602	-0.1863	-1.1967
		-0.7180	-0.5338+3.0305i	-0.5609+2.9192i	-0.6957+2.8464i	-0.4454
		-0.6949	-0.5338-3.0305i	-0.5609-2.9192i	-0.6957-2.8464i	-0.4288

system with speed governor deadband (GDB) nonlinearity. The GDB is the total amount of a sustained speed variation inside which there is no variation in the valve position. The GDB nonlinearity should be included to carry out a pragmatic AGC analysis. Speed governors in both areas shown in Fig. 2 are replaced with Fig. 3 to get transfer function model of two-area non-reheat thermal system with GDB nonlinearity. The state, control and disturbance vectors for the system are given in Eqns. (3), (8) and (10), respectively. The MATLAB program is run using data given in Appendix for 1% SLP in area-1 at $t = 0$ s. The feedback gain matrix K^* of optimal controller has dimension of [2×9] and is given as:

$$K^* = \begin{bmatrix} -0.9062 & 0.4426 & 0.8677 & 0.5168 & \cdots \\ 0.9062 & -0.0198 & -0.1169 & -0.0696 & \cdots \end{bmatrix}$$
$$\begin{bmatrix} 1.0000 & -0.0198 & -0.1169 & -0.0696 & 0.0000 \\ 0.0000 & 0.4426 & 0.8677 & 0.5168 & 1.0000 \end{bmatrix}.$$

The $\Delta F_1/\Delta F_2/\Delta Ptie_{12}$ responses of optimal controller along with that of CBPSO [8], hBFOA-PSO [7] and DE [4] optimized PI controller are shown in Figs. 8a-c and Table 3. It is observed from Figs. 8a-c and Table 3 that optimal controller shows favorable system outcomes. Furthermore, investigations of eigenvalues pattern given in Table 3 reveals that the system is stable for all four approaches as all the eigenvalues due to these controllers lie in left half of s plane. It is also observed that the real and imaginary parts of eigenvalues with optimal controller for all the system states are highly negative as compared to that of other controllers; therefore, the system with optimal controller show substantially higher stability borders with good damping. Additionally, only four complex eigenvalues are found with optimal controller while complex eigenvalues with other techniques are found six; which further aid in the stability of the system.

5.4 Two-area reheat thermal power system

The study is further extended to a two-equal area reheat thermal power system whose transfer function block diagram is shown in Fig. 4. The nominal system parameters are given in Appendix. The state, control and disturbance vectors for the system are given in Eqns. (4), (8) and (10), respectively. The power system is simulated using optimal controller with gains stated next under 1% SLP applied at $t = 0$ s in area-1.

$$K^* = \begin{bmatrix} -0.5178 & 0.4655 & 0.7736 & \cdots \\ 0.5178 & -0.0346 & -0.0767 & \cdots \end{bmatrix}$$
$$\begin{matrix} 1.8190 & -0.8046 & 1.0000 \\ 0.0328 & -0.0255 & 0.0000 \end{matrix} \quad \cdots$$
$$\begin{bmatrix} -0.0346 & -0.0767 & 0.0328 & -0.0255 & 0.0000 \\ 0.4655 & 0.7736 & 1.8190 & -0.8046 & 1.0000 \end{bmatrix}.$$

The simulation results of ΔF_1, ΔF_2 and $\Delta Ptie_{12}$ responses are shown in Figs. 9a-c and the values of various performance measures are given in Table 4.

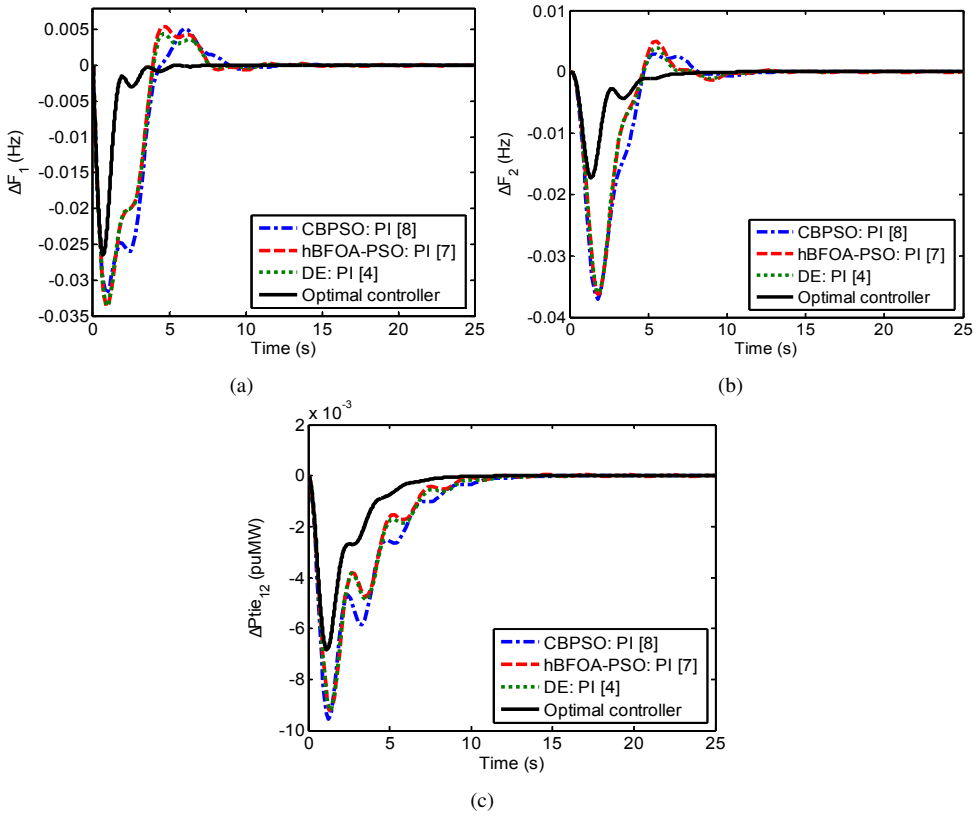

Fig. 8. Comparative dynamic responses offered by optimal controller for two-area non-reheat thermal system incorporating GDB with 1% SLP in area-1 at t = 0 s (a) ΔF_1 vs. Time, (b) ΔF_2 vs. Time and (c) $\Delta Ptie_{12}$ vs. Time.

Table 3. Comparative performance analysis of two-area non-reheat thermal system with GDB.

Parameters		Optimal controller	DE: PI [4]	CBPSO: PI [8]	hBFOA-PSO: PI [7]
PIs	ITAE	**0.1411**	0.4852	0.5765	0.5081
	IAE	**0.0772**	0.1944	0.2173	0.1981
	ITSE	**0.0009**	0.0066	0.0082	0.0068
	ISE	**0.0008**	0.0037	0.0043	0.0037
ST	ΔF_1	**4.81**	7.52	8.60	9.86
	ΔF_2	**6.27**	9.85	10.90	10.14
	$\Delta Ptie_{12}$	**5.56**	8.79	8.60	7.61
PO	ΔF_1	**0.0000**	0.0044	0.0051	0.0053
	ΔF_2	**0.0000**	0.0039	0.0028	0.0046
	$\Delta Ptie_{12}$	**0.0000**	0.0000	0.0000	0.0000
PU	ΔF_1	**-0.0265**	-0.0336	-0.0319	-0.0337
	ΔF_2	**-0.0173**	-0.0360	-0.0371	-0.0362
	$\Delta Ptie_{12}$	**-0.0068**	-0.0091	-0.0095	-0.0091
$\xi_{\min}$		**0.2418**	0.1580	0.1538	0.1617
Eigenvalues		**-7.0403**	-6.3911	-6.3981	-6.3800
		-6.9161	-6.1810	-6.1149	-6.1593
		-0.8053 ± 3.2320i	-0.4231 ± 2.6447i	-0.4479 ± 2.8780i	-0.4315 ± 2.6339i
		-1.1840 ± 2.3888i	-0.5309 ± 0.8841i	-0.4947 ± 0.7799i	-0.4837 ± 0.8753i
		-1.4537	-1.1405	-1.2790	-1.2567
		-0.6372	-0.5730 + 0.1162i	-0.5447 + 0.1257i	-0.5701 + 0.1762i
		-0.6794	-0.5730 - 0.1162i	-0.5447 - 0.1257i	-0.5701 - 0.1762i

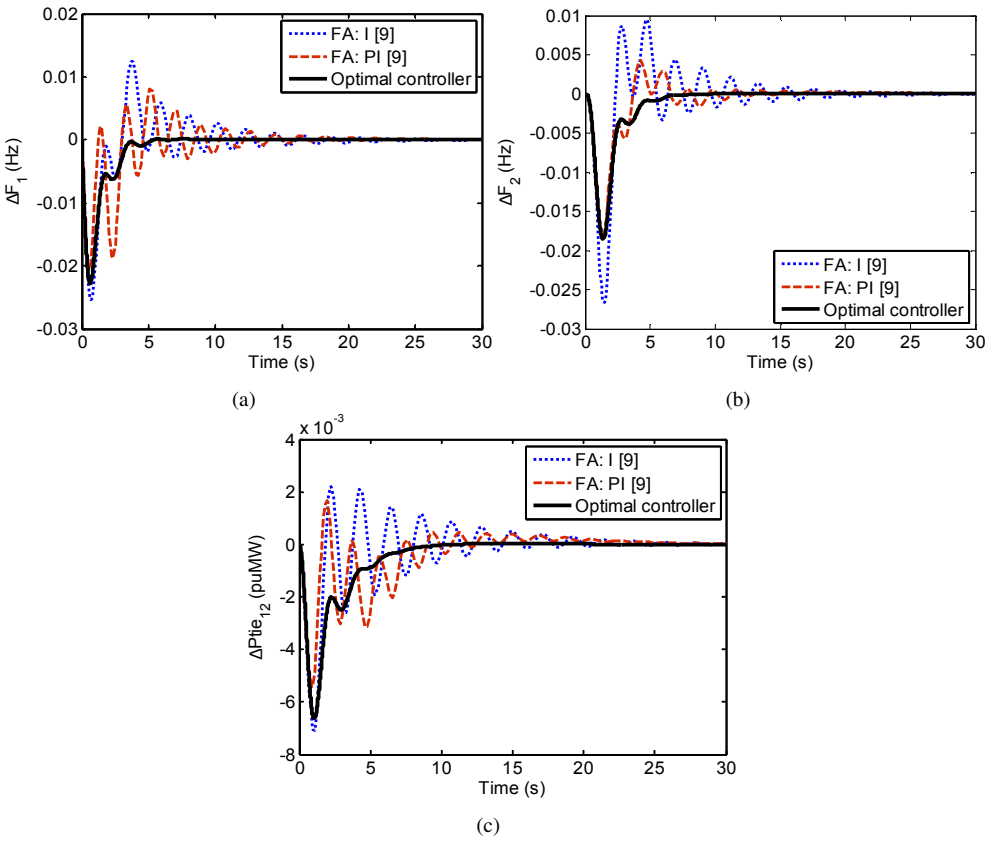

Fig. 9. Comparative dynamic responses offered by optimal controller for two-area reheat thermal system with 1% SLP in area-1 at $t = 0$ s (a) ΔF_1 vs. Time, (b) ΔF_2 vs. Time and (c) $\Delta Ptie_{12}$ vs. Time.

To demonstrate the benefit of optimal controller, results of FA tuned I/PI controller [9] for the same reheat thermal system are also incorporated in Figs. 9a-c and Table 4. The study of Figs. 9a-c reveals that the responses with optimal controller are smooth and swiftly settle in steady state to the desired zero value. It is apparent from Table 4 that lowest PIs (ITAE = 0.1576, IAE = 0.0807, ITSE = 0.0010 and ISE = 0.0008), ST ($\Delta F_1 = 4.96$ s, $\Delta F_2 = 6.08$ s and $\Delta Ptie_{12} = 5.88$ s) and PO ($\Delta F_1 = \Delta F_2 = 0$ Hz and $\Delta Ptie_{12} = 0$ puMW) values are obtained with optimal controller compared to FA based I/PI technique. The PU value of $\Delta F_1/\Delta F_2/\Delta Ptie_{12}$ response with optimal controller is observed less in comparison to FA based I ($\Delta F_1 = -0.0253$ Hz, $\Delta F_2 = -0.0266$ Hz and $\Delta Ptie_{12} = -0.0068$ puMW) controller; however, these values with optimal controller are found marginally higher ($\Delta F_1 = -0.0227$ Hz, $\Delta F_2 = -0.0186$ Hz and $\Delta Ptie_{12} = -0.0066$ puMW) compared to FA based PI ($\Delta F_1 = -0.0206$ Hz, $\Delta F_2 = -0.0180$ Hz and $\Delta Ptie_{12} = -0.0051$ puMW) technique. Though, favorable ξ_{min}/eigenvalues are obtained with the suggested controller.

5.5 Two-area hydrothermal power system with GRC/GDB

The study is also extended to a nonlinear two-area hydrothermal power system whose block diagram is given in Fig. 1 of Ref. [10]. The system contains GRC and GDB effects in thermal area only. The backlash type of GDB has a deadband width of 0.0005 [4,10] and the value of closed loop GRC nonlinearity is taken 0.1 pu/s [10,20]. The nominal parameters of the system are given in Appendix. The area-1 of the system has mechanical governor based hydro plant and area-2 is equipped with reheat type thermal plant. The state, control and disturbance vectors for the system have been given in Eqns. (5), (8) and (10), respectively. The hydrothermal system is simulated using optimal controller with gains stated next under 5% SLP applied at $t = 0$ s in area-2.

$$K^* = \begin{bmatrix} 0.9447 & 0.1733 & 0.6861 & \cdots \\ 0.3279 & 0.0362 & 0.3098 & \\ & 6.9376 & -0.6100 & -0.3814 \quad \cdots \\ & 1.3380 & 0.0131 & 0.2226 \\ -0.3279 & 0.1039 & 0.1384 & 0.1369 \quad -0.0517 \\ 0.9447 & 0.6086 & 0.9687 & 1.9148 \quad -0.8290 \end{bmatrix}. \tag{20}$$

The simulation results of ΔF_1, ΔF_2, $\Delta Ptie_{12}$, deviation in generation of area-1 (ΔP_{Gh}) and deviation in generation of area-2 (ΔP_{Gt}) system states are shown in Figs. 10a-e. To demonstrate the superiority of optimal controller, responses of GSO/PSO/SA/BA optimized PI controller [10] for the same hydrothermal system are also added in Figs. 10a-e. The study of Figs. 10a-e discloses that the responses with optimal controller are better in comparison to recently published GSO/PSO/SA/BA optimized PI controller [10]. The numerical values of various performance measures are given in Table 5. It is evident from Table 5 that lowest PIs/ST/PO/PU values are obtained with optimal controller compared to optimized PI controller. However, PU value of $\Delta Ptie_{12}$ response with optimal controller is observed slightly higher than PU values with BA based PI controller. Though, higher value of ξ_{min} (0.2315) and more negative values of seven eigenvalues out of eleven confirms the superiority of optimal controller.

From the generation response of hydro power plant in area-1 shown in Fig. 10d, it is revealed that due to non-minimum phase characteristic of hydro turbine, the response surge initially in the direction reverse to that finally directed [27]. However, response due to optimal controller settle very swiftly and with least PO/PU to the desired zero generation value in the absence of power demand in area-1. Further, from the generation response of thermal power plant in area-2 shown in Fig. 10e, it is observed that optimal controller produce more power in the transient phase with fewer oscillations and drive the state to the desired power generation of 0.05 puMW in the shortest possible time in comparison to the other controllers. Hence, in overall, it performs in the expected manner.

5.6 Three-area reheat thermal power system

To express the ability of optimal controller to cope with large and unequal multi-area interconnected power systems, the study is finally widened to an unequal three-area system having reheat thermal generating power plants in each area of the interconnected system as shown in Fig. 5. The control areas 1, 2 and 3 have ratings of 2000 MW, 5000 MW and 8000 MW, respectively. The relevant parameters of the system are given in Appendix. The state, control and disturbance vectors for the system are given in Eqns. (6), (7) and (11), respectively. A 2% SLP at $t = 0$ s is considered only in area-1 to simulate the system with optimal controller having the feedback gains matrix of [3×18] size

Table 4. Comparative performance analysis of two-area reheat thermal system.

Parameters		Optimal controller	FA: PI [9]	FA: I [9]
PIs	ITAE	**0.1576**	0.4919	0.6742
	IAE	**0.0807**	0.1137	0.1452
	ITSE	**0.0010**	0.0019	0.0029
	ISE	**0.0008**	0.0009	0.0014
ST	ΔF_1	**4.96**	16.58	17.86
	ΔF_2	**6.08**	11.79	18.77
	$\Delta Ptie_{12}$	**5.88**	8.73	13.12
PO	ΔF_1	**0.0000**	0.0076	0.0124
	ΔF_2	**0.0000**	0.0041	0.0090
	$\Delta Ptie_{12}$	**0.0000**	0.0014	0.0021
PU	ΔF_1	–0.0227	–0.0206	–0.0253
	ΔF_2	–0.0186	–0.0180	–0.0266
	$\Delta Ptie_{12}$	–0.0066	–0.0051	–0.0068
ξ_{min}		**0.2360**	0.0630	0.0567
Eigenvalues		-12.9077	-13.3033	-12.8837
		-12.9228	-12.6452	-12.9054
		-0.754 ±3.105i	-0.2122 ±3.3633i	-0.1673 ±2.9458i
		-2.3778	-2.0428 +0.2150i	-2.3368
		-0.3952	-2.0428 -0.2150i	-1.6838
		-0.2196	-0.1737 +0.1193i	-0.1493 +0.1212i
		-0.7320	-0.1737 -0.1193i	-0.1493 -0.1212i
		-1.6629 ±1.6929i	-0.4842 ±0.8488i	-0.6643 ±1.1780i
		-0.1995	-0.1923	-0.1952

Table 5. Comparative performance analysis of two-area hydrothermal system with GDB and GRC.

Parameters		Optimal Controller	PSO: PI [10]	GSO: PI [10]	SA: PI [10]	BA: PI [10]
PIs	ITAE	**1.2680**	6.8150	7.5880	10.0700	13.5200
	IAE	**0.5980**	1.4970	1.4890	1.5980	2.0080
	ITSE	**0.0812**	0.3931	0.3737	0.3662	0.5752
	ISE	**0.0460**	0.1500	0.1429	0.1204	0.1748
ST	ΔF_1	**8.64**	>100	>100	>100	>100
	ΔF_2	**8.43**	>100	>100	>100	>100
	$\Delta Ptie_{12}$	**6.35**	86.19	84.62	86.67	97.67
PO	ΔF_1	**0.0003**	0.0562	0.0073	0.0334	0.0256
	ΔF_2	**0.0021**	0.0675	0.0137	0.0402	0.0293
	$\Delta Ptie_{12}$	**0.0307**	0.0409	0.0397	0.0387	0.0406
PU	ΔF_1	**-0.1389**	-0.2119	-0.2060	-0.1862	-0.2027
	ΔF_2	**-0.1094**	-0.2124	-0.2152	-0.1694	-0.1954
	$\Delta Ptie_{12}$	-0.0115	-0.0184	-0.0171	-0.0124	0.0084
ξ_{min}		**0.2315**	0.0835	0.0890	0.0741	0.0817
Eigenvalues		-12.9152	-12.8745	-12.9167	-12.9001	-12.8633
		-0.6597±2.7725i	-0.2116±2.5258i	-0.2283±2.5556i	-0.2025±2.7245i	-0.2189±2.6700i
		-2.7644	-3.0667	-3.1127	-2.7542	-2.7643
		-1.9260	-2.3483	-2.4053	-1.9697	-2.0404
		-0.9225±1.0374i	-0.2905±0.9639i	-0.3144±1.1532i	-0.6332±0.5978i	-0.6643±0.5547i
		-0.6705	-0.3071	-0.0868	-0.3987	-0.2745
		-0.1725±0.0942i	-0.0787±0.1124i	-0.0654±0.0339i	-0.0312±0.0790i	-0.0323±0.0795i
		-0.1998	-0.1891	-0.2095	-0.1907	-0.1739

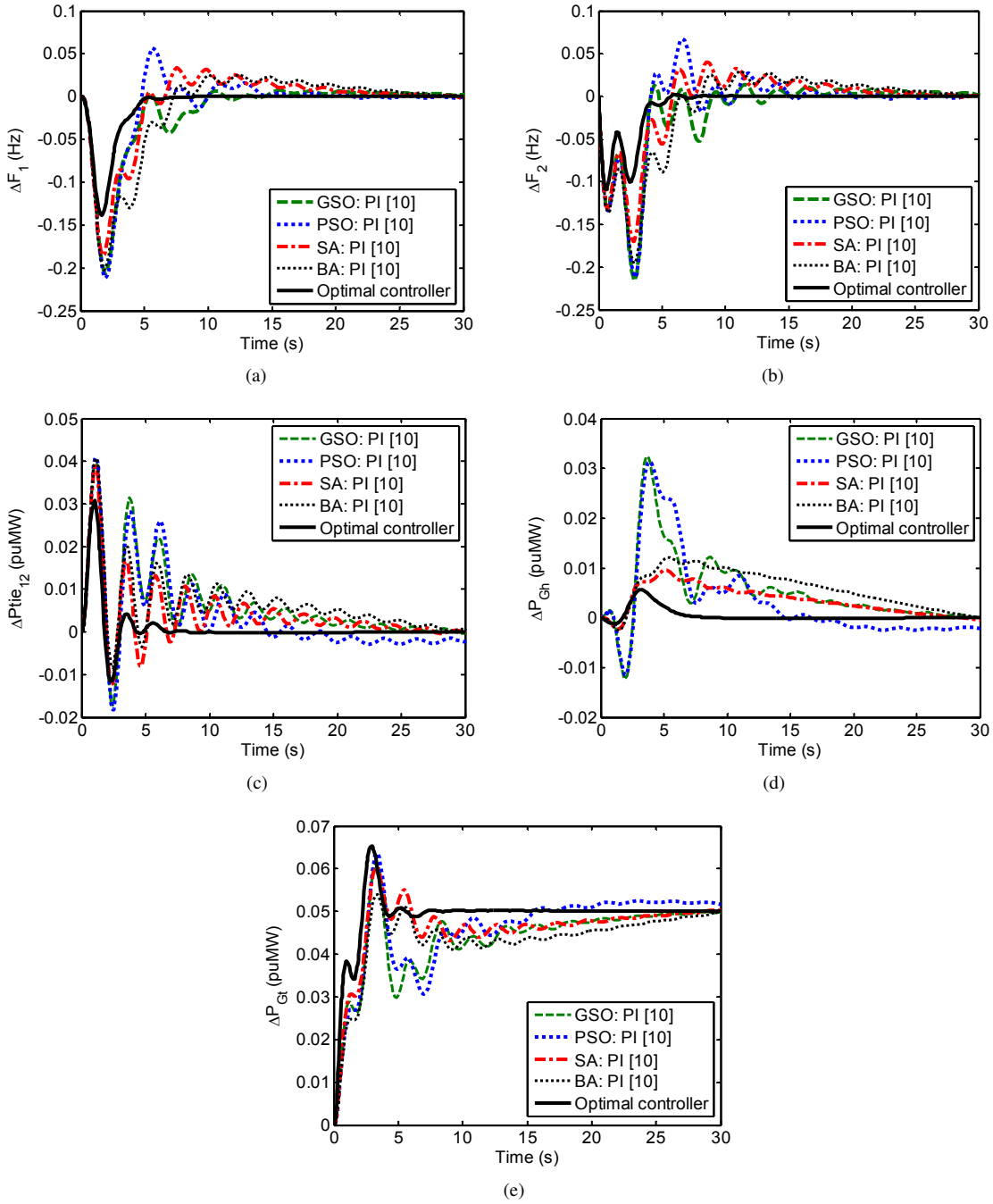

Fig. 10. Comparative dynamic responses offered by optimal controller for two-area hydrothermal system incorporating GDB and GRC with 5% SLP in area-2 at t = 0 s (a) ΔF_1 vs. Time, (b) ΔF_2 vs. Time, (c) $\Delta Ptie_{12}$ vs. Time, (d) ΔP_{Gh} vs. Time and (e) ΔP_{Gt} vs. Time.

stated as follows:

$$K^* = \begin{bmatrix} 0.4725 & -0.0132 & -0.0338 & -0.5409 & \cdots \\ -0.0812 & 0.4999 & 0.0277 & 0.2184 & \\ -0.0591 & -0.0281 & 0.5129 & 0.0484 & \end{bmatrix}$$
$$\begin{matrix} -0.5098 & 0.0776 & 0.8081 & -0.0773 & -0.0792 \\ -0.0028 & -0.5530 & -0.1019 & 0.8362 & -0.0147 \\ 0.1651 & 0.2917 & -0.0889 & -0.0332 & 0.8407 \end{matrix} \cdots$$
$$\begin{matrix} 1.7877 & -0.0152 & -0.0036 & -0.7850 & -0.0032 \\ 0.0180 & 1.8186 & 0.0249 & -0.0198 & -0.7969 \\ 0.0264 & 0.0555 & 1.8416 & -0.0232 & -0.0305 \end{matrix} \cdots$$
$$\begin{bmatrix} -0.0083 & 0.9997 & 0.0107 & -0.0206 \\ -0.0152 & -0.0105 & 0.9999 & 0.0099 \\ -0.8078 & 0.0207 & -0.0097 & 0.9997 \end{bmatrix}.$$

The ΔF_1, ΔF_2, ΔF_3, deviation in area-1 tie-line ($\Delta Ptie_1$), deviation in area-2 tie-line ($\Delta Ptie_2$) and deviation in area-3 tie-line ($\Delta Ptie_3$) responses of the three-area system and the comparative performance parameters with optimal controller are shown in Figs. 11a-f and Table 6, respectively. For evaluation reason, corresponding results and numerical values with MFO [12]/KHA [14] tuned PI controller are also shown in same Fig. 11 and Table 6. The examination of the dynamic responses shown in Fig. 11 clearly states that appreciably better responses in terms of negligible oscillations, less PO/PU are obtained with optimal controller compared to MFO [12]/KHA [14] tuned PI controller. Table 6 also focuses on the superiority of optimal controller in terms of least PIs/ST/PO/PU, higher ξ_{min} and more negative real parts of fourteen number of eigenvalues out of total eighteen number of eigenvalues.

6 SENSITIVITY ANALYSIS

The above discussions consolidate that optimal controller is established to be the best controller. However, this controller should work robustly under changes in the system parameters and initial loading condition. Therefore, a sensitivity analysis is carried out to check the potential/robustness of the optimal controller against wide changes in the initial loading condition and nominal system parameters [5,7-8,13,16-18,20,22,24-26]. Fig. 12a shows ΔF response at nominal and $\pm 25\%$ variation in initial system loading from its nominal 50% initial system loading for single-area multi-source system, Fig. 12b shows ΔF_1 response at nominal and $\pm 25\%$ variation in nominal T_{SG} parameter for two-area non-reheat thermal system, Fig. 12c shows $\Delta Ptie_{12}$ response at nominal and $\pm 25\%$ variation in nominal R parameter for two-area non-reheat thermal system with GDB, Fig. 12d shows ΔF_2 response at nominal and $\pm 25\%$ variation in nominal T_T parameter for two-area reheat thermal system, Fig. 12e shows ΔF_1 response at nominal and $\pm 25\%$ simultaneous variation in nominal T_{GH}, T_{RS}, T_{RH} and T_W parameters for two-area hydrothermal system and Fig. 12e shows ΔF_3 response at nominal and $\pm 25\%$ simultaneous variation in nominal K_R, T_T, K_{PS} and T_{PS} parameters for three-area reheat thermal system. Critical assessment of all frequency and tie-line responses visibly reveals that all responses are more or less identical. Only six sample responses are shown in Fig. 12 to justify the statement. Therefore, the optimum values of K^* matrix of optimal controller obtained at the nominal parameters and nominal initial loading of 50% need not be reset for extensive alteration in the initial loading of the system or system parameters.

7 CONCLUSION

In this work, a critical comparative performance investigation of optimal controller with various intelligent soft computing techniques based control schemes published recently in the literature is performed for AGC analysis of some single/multi-area power system models. Modern optimal control theory is effectively utilized as a control strategy to estimate the full state feedback gains of optimal controller which assists to bring the power system to its normal operating condition following step load perturbations in one or all control areas. The AGC performance examination initiates with single-area multi-source hydrothermal gas system with GRC effect, proceed to two-area non-reheat thermal power system, two-area non-reheat thermal power system with GDB, two-area reheat thermal power system, two-area hydrothermal power system with GDB/GRC and, then extended to three-area reheat thermal power system. The simulation results reflect that optimal controller provides enriched dynamic performances than various published techniques for both single and multi-area power system models in terms of minimum oscillations, less numerical values of settling time, peak overshoot, peak undershoot, various performance indices and, higher numerical values of minimum damping ratio. The eigenvalues study substantiates the higher stability margin of the systems under study with optimal controller compared to other prevalent methods. The sensitivity analysis demonstrates the robustness of optimal gains of optimal controller for extensive variations in the initial loading and several parameters of the systems. Thus, optimal controller may be employed in power systems to improve the AGC performance remarkably by decimating the effects of SLP in the control areas.

APPENDIX: SYSTEMS DATA

Single-area multi-source power system [11]:
$P_r = 2000$ MW, $F^0 = 60$ Hz, $K_{PS} = 68.9566$ Hz/puMW, $T_{PS} = 11.49$ s, $T_{SG} = 0.08$ s,

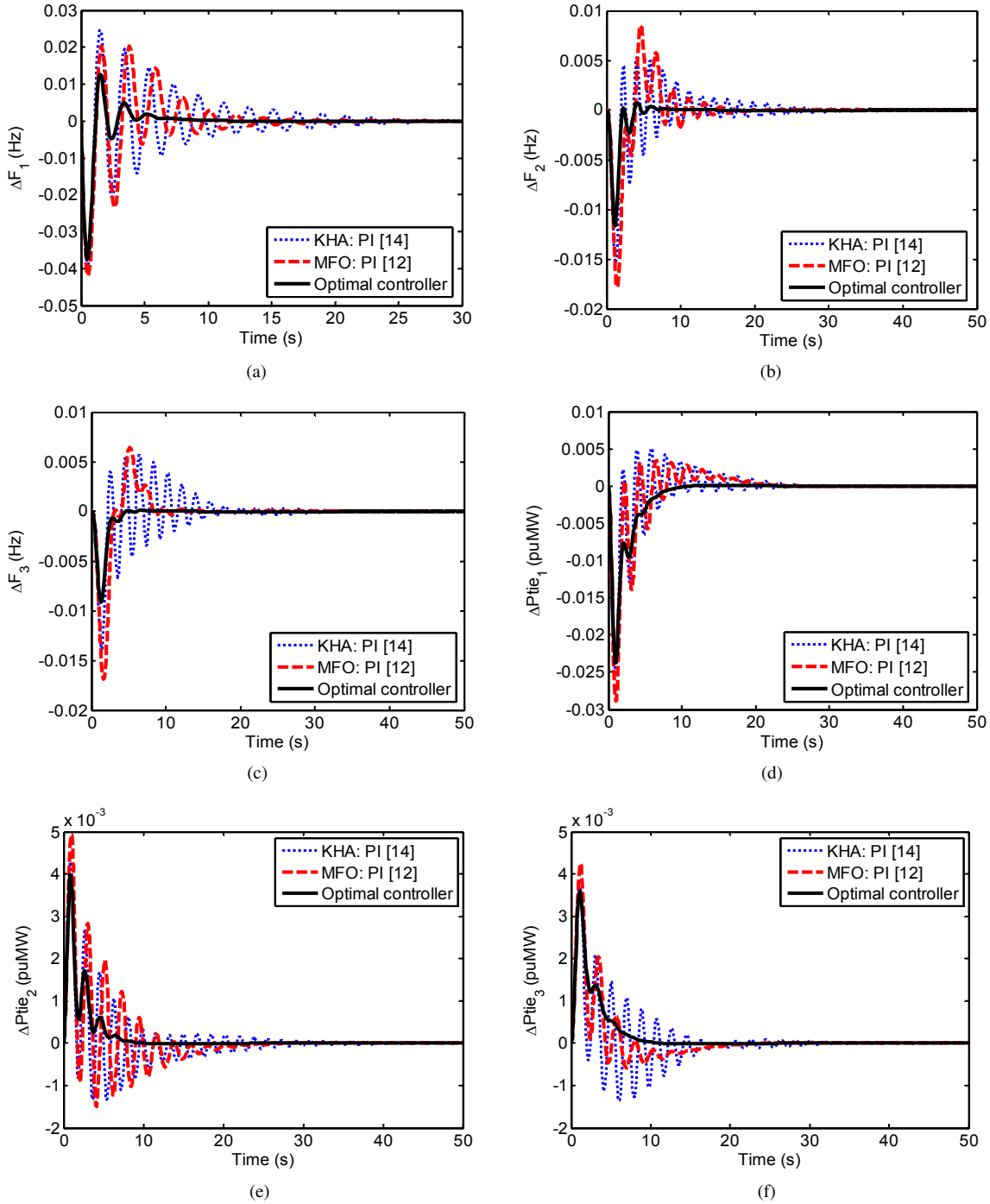

Fig. 11. Comparative dynamic responses offered by optimal controller for three-area reheat thermal system with 2% SLP in area-1 at $t = 0$ s (a) ΔF_1 vs. Time, (b) ΔF_2 vs. Time, (c) ΔF_3 vs. Time, (d) $\Delta Ptie_1$ vs. Time, (e) $\Delta Ptie_2$ vs. Time and (f) $\Delta Ptie_3$ vs. Time.

Table 6. Comparative performance analysis of three-area reheat thermal system.

Parameters		Optimal controller	MFO: PI [12]	KHA: PI [14]
PIs	ITAE	**0.2731**	1.1300	1.6460
	IAE	**0.1280**	0.2720	0.2926
	ITSE	**0.00133**	0.00662	0.00712
	ISE	**0.00136**	0.00319	0.00277
ST	ΔF_1	**7.68**	17.78	24.83
	ΔF_2	**4.39**	13.53	22.61
	ΔF_3	**4.09**	8.13	16.27
PO	ΔF_1	**0.0127**	0.0203	0.0246
	ΔF_2	**0.0007**	0.0084	0.0053
	ΔF_3	**0.0000**	0.0064	0.0056
PU	ΔF_1	**-0.0374**	-0.0420	-0.0397
	ΔF_2	**-0.0170**	-0.0179	-0.0154
	ΔF_3	**-0.0091**	-0.0169	-0.0139
$\xi_{\min}$		**0.2164**	0.0816	0.0318
Eigenvalues		-12.9087	-12.7693	-13.2691
		-12.9047	-12.8270	-13.1862
		-12.9227	-12.8032	-12.9061
		-0.7429 ±3.3523i	-0.2429 ±2.9670i	-0.1138 ±3.5779i
		-0.7854 ± 3.0397i	-0.2817 ±2.6872i	-0.1568 ±3.2313i
		-1.6761 ± 1.6732i	-0.4578 ±0.7661i	-1.1867 ±2.2744i
		-2.4892	-2.3216	-2.4421
		-2.3376	-2.3184	-0.2111
		-0.7376	-2.0980	-2.3420
		-0.3969	-0.1925	-0.1277
		-0.3812	-0.1958 +0.1658i	-0.2669 +0.0935i
		-0.2218	-0.1958 -0.1568i	-0.2669 -0.0935i
		-0.2194	-0.1320 +0.1437i	-0.0081
		-0.1995	-0.1320 -0.1437i	-0.0090
		0.0000	0.0000	0.0000

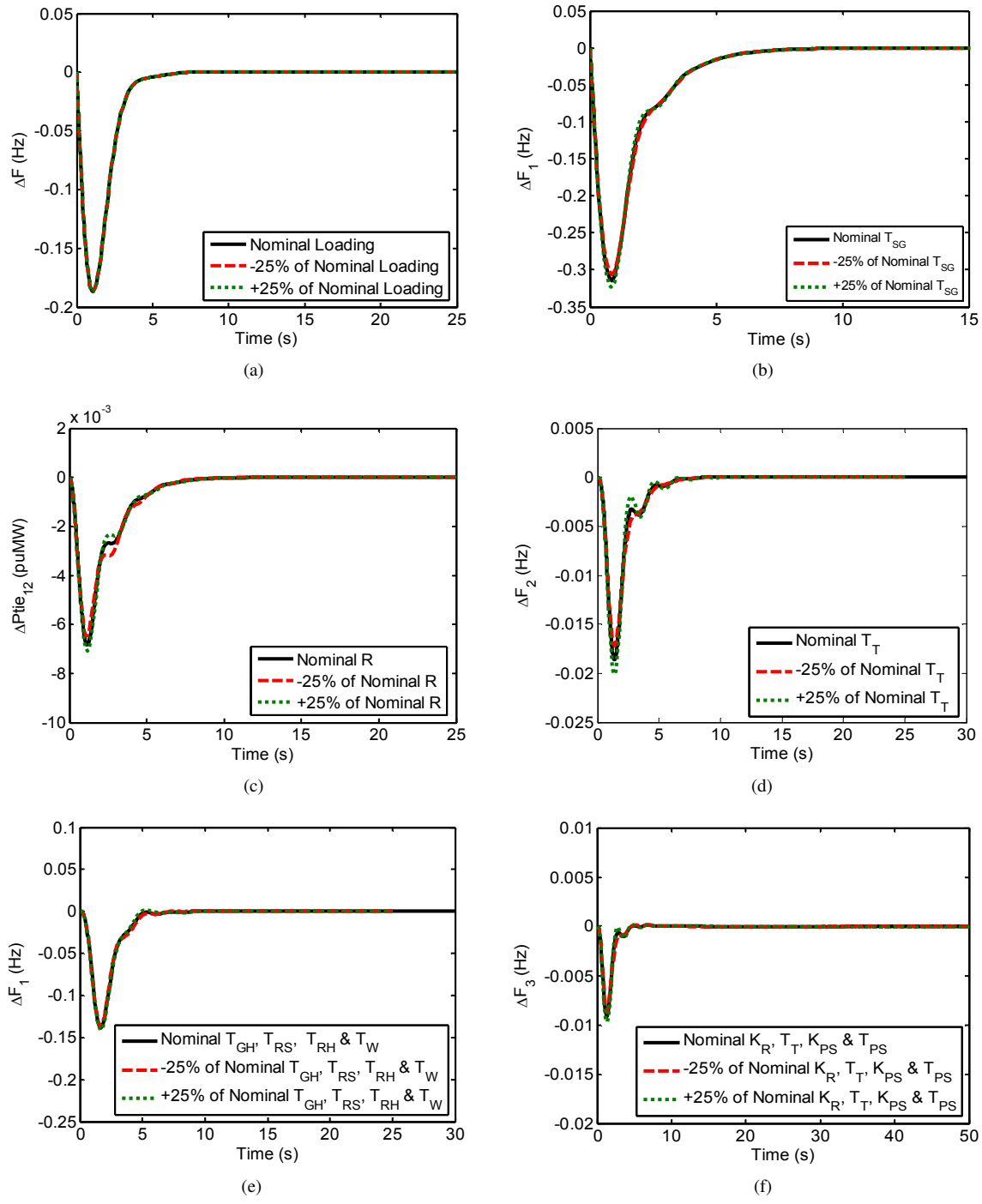

Fig. 12. System dynamic responses with optimal controller during sensitivity analysis (a) ΔF vs. Time of single-area multi-source system, (b) ΔF_1 vs. Time of two-area non-reheat thermal system, (c) $\Delta Ptie_{12}$ vs. Time two-area non-reheat thermal system with GDB, (d) ΔF_2 vs. Time of two-area reheat thermal system, (e) ΔF_1 vs. Time of two-area hydrothermal system and (f) ΔF_3 vs. Time of three-area reheat thermal system.

$K_R = 0.3$, $T_R = 10$ s, $T_T = 0.3$ s, $R = 2.4$ Hz/puMW, $T_{GH} = 0.2$ s, $T_{RS} = 5$ s, $T_{RH} = 28.75$ s, $T_W = 1$ s, $\alpha_{TH} = 0.543478$, $\alpha_{HY} = 0.326084$, $\alpha_G = 0.130438$, $X_G = 0.6$ s, $Y_G = 1$ s, $a = 1$, $c_g = 1$, $b_g = 0.05$ s, $T_F = 0.23$ s, $T_{CR} = 0.01$ s, $T_{CD} = 0.2$ s, initial loading = 92%.

Two-area non-reheat thermal power system [5,7]:

$P_{ri} = 2000$ MW, $F^0 = 60$ Hz, $K_{PSi} = 120$ Hz/puMW, $T_{PSi} = 20$ s, $T_{SGi} = 0.08$ s, $T_{Ti} = 0.3$ s, $R_i = 2.4$ Hz/puMW, $\beta_i = 0.425$ puMW/Hz, $2\pi T_{12} = 0.545$ puMW/Hz, $\alpha_{12} = -1$, initial loading = 50%.

Two-area non-reheat thermal power system with GDB [4,7-8]:

$P_{ri} = 2000$ MW, $F^0 = 60$ Hz, $K_{PSi} = 120$ Hz/puMW, $T_{PSi} = 20$ s, $T_{SGi} = 0.2$ s, $T_{Ti} = 0.3$ s, $R_i = 2.4$ Hz/puMW, $\beta_i = 0.425$ puMW/Hz, $T_{12} = 0.0707$ puMW/rad, $\alpha_{12} = -1$, $N_1 = 0.8$, $N_2 = -0.2$, $\omega_0 = \pi$, initial loading = 50%.

Two-area reheat thermal power system [9]:

$P_{ri} = 2000$ MW, $F^0 = 60$ Hz, $K_{PSi} = 120$ Hz/puMW, $T_{PSi} = 20$ s, $T_{SGi} = 0.08$ s, $K_{Ri} = 0.5$, $T_{Ri} = 10$ s, $T_{Ti} = 0.3$ s, $R_i = 2.4$ Hz/puMW, $\beta_i = 0.425$ puMW/Hz, $2\pi T_{12} = 0.5438$ puMW/Hz, $\alpha_{12} = -1$, initial loading = 50%.

Two-area reheat hydrothermal power system [10]:

$F^0 = 60$ Hz, $K_{PS1} = 20$ Hz/puMW, $T_{PS1} = 3.76$ s, $T_{GH} = 0.6$ s, $T_{RS} = 5$ s, $T_{RH} = 32$ s, $T_W = 1$ s, $K_{PS2} = 120$ Hz/puMW, $T_{PS2} = 20$ s, $T_{SG} = 0.08$ s, $K_R = 0.5$, $T_R = 10$ s, $T_T = 0.3$ s, $R_1 = 3$ Hz/puMW, $\beta_1 = 0.313$ puMW/Hz, $R_2 = 2.4$ Hz/puMW, $\beta_2 = 0.425$ puMW/Hz, $2\pi T_{12} = 0.545$ puMW/Hz, $\alpha_{12} = -1$.

Three-area reheat thermal power system [12,14]:

$P_{r1} = 2000$ MW, $P_{r2} = 5000$ MW, $P_{r3} = 8000$ MW, $F^0 = 60$ Hz, $\beta_i = 0.425$ pu MW/Hz, $R_i = 2.4$ Hz/pu MW, $T_{SGi} = 0.08$ s, $T_{Ti} = 0.3$ s, $K_{Ri} = 0.5$, $T_{Ri} = 10$ s, $K_{PSi} = 120$ Hz/puMW, $T_{PSi} = 20$ s, $2\pi T_{12} = 2\pi T_{13} = 2\pi T_{23} = 0.5441$ pu MW/Hz, $\alpha_{12} = -2/5$, $\alpha_{13} = -2/8$, $\alpha_{23} = -5/8$, initial loading = 50%.

REFERENCES

[1] O. I. Elgerd, *Electric Energy Systems Theory: An Introduction*. 2nd ed. 42nd reprint. New Delhi: McGraw Hill Education 2014; 299–362.

[2] Ibraheem, P. Kumar and D. P. Kothari, "Recent philosophies of automatic generation control strategies in power systems. *IEEE Trans. Power Syst.*, vol. 20, no. 1, pp. 346–357, Feb. 2005.

[3] R. Shankar, S. R. Pradhan, K. Chatterjee and R. Mandal, "A comprehensive state of the art literature survey on LFC mechanism for power system," *Renewab. Sustainab. Energy Reviews*, vol. 76, no. 6, pp. 1185–1207, Sep. 2017.

[4] B. Mohanty, S. Panda and P. K. Hota, "Differential evolution algorithm based automatic generation control for interconnected power systems with non-linearity," *Alexandria Eng. J.*, vol. 53, no. 3, pp. 537–552, Sep. 2014.

[5] R. K. Sahu, S. Panda, U. K. Rout and D. K. Sahoo, "Teaching learning based optimization algorithm for automatic generation control of power system using 2-DOF PID controller," *Int. J. Elect. Power Energy Syst.*, vol. 77, pp. 287–301, May 2016.

[6] S. D. Madasu, M. L. S. S. Kumar and A. K. Singh, "Comparable investigation of backtracking search algorithm in automatic generation control for two area reheat interconnected thermal power system," *Applied Soft Comput.*, vol. 55, pp. 197–210, Jun. 2017.

[7] S. Panda, B. Mohanty and P. K. Hota, "Hybrid BFOA-PSO algorithm for automatic generation control of linear and nonlinear interconnected power systems," *Applied Soft Comput.*, vol. 13, no. 12, pp. 4718–4730, Dec. 2013.

[8] H. Gozde and M. C. Taplamacioglu, "Automatic generation control application with craziness based particle swarm optimization in a thermal power system," *Int. J. Elect. Power Energy Syst.*, vol. 33, no. 1, pp. 8–16, Jan. 2011.

[9] T. S. Gorripotu, R. K. Sahu and S. Panda, "Comparative performance analysis of classical controllers in LFC using FA technique, " In *Proc. of 2015 Int. Conf. on Electrical, Electronics, Signals, Communication and Optimization (EESCO)*, Visakhapatnam, India, 2015, p. 1–5.

[10] K. K. Baral, A. K. Barisal and B. Mohanty, "Load frequency controller design via GSO algorithm for nonlinear interconnected power system, " In Proc. of *2016 Int. Conf. on Signal Processing, Communication, Power and Embedded System (SCOPES)*, Paralakhemundi, Odisha, India, 2016, p. 662–668.

[11] R. Sivalingam, S. Chinnamuthu and S. S. Dash, "A hybrid stochastic fractal search and local unimodal sampling based multistage PDF plus (1 + PI) controller for automatic generation control of power systems," *J. Franklin Inst.*, vol. 354, no. 12, pp. 4762–4783, Aug. 2017.

[12] D. K. Lal, K. K. Bhoi and A. K. Barisal, "Performance evaluation of MFO algorithm for AGC of a multi area power system, " In Proc. of *2016 Int. Conf. on Signal Processing, Communication, Power and Embedded System (SCOPES)*, Paralakhemundi, Odisha, India, 2016, p. 903-908.

[13] J. Morsali, K. Zare and M. T. Hagh, "Applying fractional order PID to design TCSC-based damping controller in coordination with automatic generation control of interconnected multi-source power system," *Eng. Sc. Tech. an Int. J.*, vol. 20, no. 1, pp. 1–17, Feb. 2017.

[14] D. Guha, P. K. Roy and S. Banerjee, "Application of krill herd algorithm for optimum design of load frequency controller for multi-area power system network with generation rate constraint," In *Proc. of the 4th Int. Conf. on Frontiers in Intelligent Computing: Theory and Applications (FICTA)*, 2015, p. 245-257.

[15] T. Mahto and V. Mukherjee, "A novel scaling factor based fuzzy logic controller for frequency control of an isolated hybrid power system," *Energy*, vol. 130, pp. 339–350, Jul. 2017.

[16] Y. Arya, "AGC performance enrichment of multi-source hydrothermal gas power systems using new optimized FOF-PID controller and redox flow batteries," *Energy*, vol. 127, pp. 704–715, May 2017.

[17] Y. Arya and N. Kumar, "Design and analysis of BFOA-optimized fuzzy PI/PID controller for AGC of multi-area traditional/restructured electrical power systems," *Soft Comput.*, vol. 21, no. 21, pp. 6435–6452, Nov. 2017.

[18] B. K. Sahu, S. Pati and S. Panda, "Hybrid differential evolution particle swarm optimisation optimised fuzzy proportional-integral derivative controller for automatic generation control of interconnected power system," *IET Gener. Transm. Distrib.*, vol. 8, no. 11, pp. 1789–1800, Nov. 2014.

[19] P. Bhatt, S. P. Ghoshal and R. Roy, "Load frequency stabilization by coordinated control of thyristor controlled phase shifters and superconducting magnetic energy storage for three types of interconnected two-area power systems," *Int. J. Elect. Power Energy Syst.*, vol. 32, no. 10, pp. 1111–1124, Dec. 2010.

[20] Y. Arya, "AGC of restructured multi-area multi-source hydrothermal power systems incorporating energy storage units via optimal fractional-order fuzzy PID controller," *Neural Comput. Appl.*, Jul. 2017, DOI 10.1007/s00521-017-3114-5.

[21] C. E. Fosha and O. I. Elgerd, "The megawatt-frequency control problem: a new approach via optimal control theory," *IEEE Trans. Power App. Syst.*, vol. PAS-89, no. 4, pp. 563–577, Apr. 1970.

[22] Y. Arya and N. Kumar, AGC of a multi-area multi-source hydrothermal power system interconnected via AC/DC parallel links under deregulated environment," *Int. J. Elect. Power Energy Syst.*, vol. 75, pp. 127–138, Feb. 2016.

[23] Ibraheem, Nizamuddin and T. S. Bhatti, "AGC of two area power system interconnected by AC/DC links with diverse sources in each area," *Int. J. Elect. Power Energy Syst.*, vol. 55, pp. 297–304, Feb. 2014.

[24] Y. Arya, N. Kumar and Ibraheem, "AGC of a two-area multi-source power system interconnected via AC/DC parallel links under restructured power environment," *Optimal Contr. Appl. Methods*, vol. 37, no. 4, pp. 590–607, Jul.-Aug. 2016.

[25] Y. Arya and N. Kumar, "Optimal AGC with redox flow batteries in multi-area restructured power systems," *Eng. Sc. Tech. an Int. J.*, vol. 19, no. 3, pp. 1145–1159, Sep. 2016.

[26] Y. Arya, N. Kumar and S. K. Gupta, "Load frequency control of a four-area power system using linear quadratic regulator," *Int. J. Energy Sc.*, vol. 2, no. 2, pp. 69–76, Apr. 2012.

[27] Y. Arya and N. Kumar, "Optimal control strategy-based AGC of electrical power systems: A comparative performance analysis," *Optimal Contr. Appl. Methods*, Jan. 2017, DOI: 10.1002/oca.2304.

[28] M. L. Kothari and J. Nanda, "Application of optimal control strategy to automatic generation control of a hydrothermal system," *IEE Proc. Control Theory Appl.*, vol. 135, pt. D, no.4, pp. 268–274, Jul. 1988.

[29] N. Hasan, Ibraheem and P. Kumar, "Optimal automatic generation control of interconnected power system considering new structures of matrix Q," *Elect. Power Compon. Syst.*, vol. 41, no. 2, pp. 136–156, Jan. 2013.

[30] B. D. O. Anderson and J. B. More, *Optimal Control: Linear Quadratic Methods*, Prentice Hall of India, 1991.

Pankaj Dahiya received his B.Tech. in electronics and instrumentation engineering from Kurukshetra university, Kurukshetra, Haryana, India, and finished his M.Tech. in electrical engineering (instrumentation & control) from Deenbandhu Chhotu Ram university of science & technology, Murthal, Haryana, India, in 2006 and 2009, respectively. He is currently working towards his Ph.D. in the Department of electrical and electronics engineering, National institute of technology, Delhi, New Delhi, India. His research of interest includes stability analysis and advanced control applications in power systems.

Pankaj Mukhija is currently working as an assistant professor in the Department of electrical and electronics engineering at National institute of technology, Delhi, India. He received his Ph.D. from Indian institute of technology, Delhi in 2013. His research interest covers control of networked systems and time-delay systems.

Anmol Ratna Saxena was born in Sagar, M.P., India in 1978. He received diploma in engineering from Govt. polytechnic Nowgong, India in 1997, bachelor of engineering degree from Bhilai institute of technology, Bhilai, India in 2000 and master's degree from Maulana Azad national institute of technology, Bhopal, India in 2007, all in electrical engineering. He received Ph.D. degree from Indian institute of technology Delhi, India in 2014. From 2013 to 2014, he has worked as assistant professor at Madhav institute of technology and science, Gwalior, India. Since December 2014, he has been with the Department of electrical and electronics engineering at National institute of technology, Delhi, India, where he is currently acting as an assistant professor. His research interests include design of power electronic converters, DC-DC converters for point of load applications, digital control, modelling and robust control design of DC-DC converters.

Yogendra Arya received his A.M.I.E. in electrical engineering from The institution of engineers (India), in 2008 and his master's degree in electrical engineering (instrumentation & control) from Deenbandhu Chhotu Ram university of science & technology, Murthal, Haryana, India, in 2010. He has submitted his Ph.D. thesis in Delhi technological university, Delhi, India. He is currently working as an assistant professor with the Department of electrical and electronics engineering, Maharaja Surajmal institute of technology in New Delhi. He is an associate member of The institution of engineers (India). His broad area of interest includes operation and control of power system.

AUTHORS' ADDRESSES

Pankaj Dahiya, M.Tech.
Asst. Prof. Pankaj Mukhija, Ph.D.
Asst. Prof. Anmol Ratna Saxena, Ph.D.
Department of Electrical and Electronics Engineering,
National Institute of Technology,
Sector A-7, Institutional Area, Narela, Delhi-110040, India
email: {pankajdahiya,
pankajmukhija,anmolsaxena}@nitdelhi.ac.in

Asst. Prof. Yogendra Arya, M.Tech.
Department of Electrical and Electronics Engineering,
Maharaja Surajmal Institute of Technology,
C-4, Janakpuri, New Delhi-110058, India
email: mr.y.arya@gmail.com

Received: 2016-02-23
Accepted: 2017-08-06